Materials and Design 63 (2014) 460–463

Contents lists available at ScienceDirect

Materials and Design

journal homepage: www.elsevier.com/locate/matdes

Short Communication

High damping NiTi/Ti_3Sn in situ composite with transformation-mediated plasticity

Junsong Zhang [a], Yinong Liu [b], Yong Huan [c], Shijie Hao [a], Daqiang Jiang [a], Yang Ren [d], Yang Shao [a], Yadong Ru [a], Zhongqiang Wang [a], Lishan Cui [a,*]

[a] Department of Materials Science and Engineering, China University of Petroleum-Beijing, Changping, Beijing 102249, China
[b] School of Mechanical and Chemical Engineering, The University of Western Australia, Crawley, WA 6009, Australia
[c] State Key Laboratory of Nonlinear Mechanics (LNM), Institute of Mechanics, Chinese Academy of Sciences, Beijing 100190, China
[d] X-ray Science Division, Argonne National Laboratory, Argonne, IL 60439, USA

ARTICLE INFO

Article history:
Received 6 March 2014
Accepted 28 May 2014
Available online 6 June 2014

Keywords:
Composite
Synchrotron
Damping
Ti_3Sn
NiTi

ABSTRACT

The concept of transformation-induced plasticity effect is introduced in this work to improve the plasticity of brittle intermetallic compound Ti_3Sn, which is a potent high damping material. This concept is achieved in an in situ NiTi/Ti_3Sn composite. The composite is composed of primary Ti_3Sn phase and (NiTi + Ti_3Sn) eutectic structure formed via hypereutectic solidification. The composite exhibits a high damping capacity of 0.075 (indexed by $\tan\delta$), a high ultimate compressive strength of 1350 MPa, and a large plasticity of 27.5%. In situ synchrotron high-energy X-ray diffraction measurements revealed clear evidence of the stress-induced martensitic transformation (B2 → B19′) of the NiTi component during deformation. The strength of the composite mainly stems from the Ti_3Sn, whereas the NiTi component is responsible for the excellent plasticity of the composite.

1. Introduction

High damping materials are used in various fields to eliminate noise, to reduce mechanical vibration, and to protect buildings against earthquake [1–7]. The combination of high damping capacity and good mechanical properties is very important for structural applications. However, these properties are often incompatible in metals, because of the trade-off relations between strength and damping [1,2]. Therefore, it is of interest to search and develop new damping materials that can simultaneously couple high damping capacity and excellent mechanical performances.

Recently, Ti_3Sn intermetallic compound has been reported to exhibit exceptionally high damping capacity [8], raising high expectations for innovative applications. The maximum damping capacity of Ti_3Sn has been reported to reach 0.2 (indexed by $\tan\delta$) [8], which is over four times higher than those of typical commercial Mn–Cu-based high-damping alloys (with $\tan\delta$ of about 0.05) [9,10] and NiTi shape memory alloys ($\tan\delta$ approximate 0.04) [11,12]. However, due to the lack of adequate slip systems in its $D0_{19}$ crystal structure, the Ti_3Sn intermetallic compound is extremely brittle [13,14]. This severely restricts its practical application.

Inspired by the transformation-induced plasticity effect in quenching–partitioning martensitic steels, in which the residual austenite is used to improve the ductility of the martensite [15–17], we attempt to explore a new toughening mechanism by introducing a phase transforming component to form a composite with the high damping but brittle Ti_3Sn intermetallic compound for excellent mechanical properties as well as high damping capacity. An ideal candidate for this phase transforming component is NiTi shape memory alloy, which deforms by stress-induced martensitic transformation (SIMT) [18,19]. Our *Science* paper has proposed that the atomic-level transformation strain of NiTi is only ~10% after SIMT [19,20]. In comparison, the inelastic strain between two adjacent atomic planes approaches 100% at a dislocation in conventional metal [20,21]. The NiTi shape memory alloy is expected to prevent stress concentration and strain localization, which may optimize the mechanical properties of the composite. NiTi and Ti_3Sn can form a pseudo binary eutectic solidification at approximately 30% volume fraction of NiTi [22], providing an ideal condition to form ultrafine lamellar in situ composite.

2. Experimental procedure

An alloy ingot (7 kg) with a nominal composition of $Ti_{69}Ni_{11}Sn_{20}$ (at. %) was produced from high-purity elemental metals (purity

* Corresponding author. Tel.: +86 10 89733975.
E-mail address: lscui@cup.edu.cn (L. Cui).

http://dx.doi.org/10.1016/j.matdes.2014.05.062
0261-3069/

>99.8 wt.%) by vacuum induction melting. Test samples cut from the ingot were annealed in vacuum at 950 °C for 10 h. The microstructure of the composite ingot was characterized by means of X-ray diffraction (XRD, Bruker AXS D8 instrument) and scanning electron microscopy (SEM, FEI Quanta 200F instrument). The damping capacity of the composite was measured using a dynamic mechanical analyzer (DMA, TA Q800) in three-point bending mode with an amplitude of 5 μm. The geometry of the damping specimens was 1 × 2 × 40 mm, and the damping tests were conducted at a frequency of 1 Hz in the temperature range of −130 °C to 300 °C with a constant heating rate of 3 °C/min. Differential scanning calorimetry (DSC) experiment was conducted using a TA INST2910 differential scanning calorimeter with a heating/cooling rate of 10 °C/min. Cylindrical specimens of 5 mm in diameter and 10 mm in length were prepared and tested for mechanical behavior using a MTS810 material test system under quasistatic compressive loading at an initial strain rate of 1×10^{-3} s^{-1} at room temperature. In situ synchrotron high-energy X-ray diffraction (HEXRD) measurements during compression were performed at the 11-ID-C beam line of the Advanced Photon Source, Argonne National Laboratory, USA. High-energy X-rays with a beam size of 0.6 mm × 0.6 mm and wavelength of 0.10798 Å was used to obtain two-dimensional (2D) diffraction patterns in transmission geometry.

3. Results and discussion

Fig. 1 shows an XRD spectrum ((a)) and SEM backscattered electron micrographs ((b) and (c)) of the NiTi/Ti_3Sn composite. The composite contains a mixture of monoclinic $P2_1/m$ NiTi (B19′), body-centered cubic (bcc) Pm3m NiTi (B2) and hexagonal $P6_3/mmc$ Ti_3Sn (D019) intermetallic phases. The composite has a hypereutectic microstructure consisting of primary Ti_3Sn dendrites (the bright phase) and an ultrafine eutectic structure (the gray structure), as seen in Fig. 1(b). Fig. 1(c) shows the eutectic structure at a higher magnification. It is composed of Ti_3Sn (bright) and NiTi (black) phases in a lamellar structure. The Ti_3Sn lamellar spacing in the eutectic structure is about 400–1000 nm. Quantitative image analysis of SEM micrographs shows that the phase volume fraction of the pre-eutectic Ti_3Sn is about 80%.

Fig. 2(a) reveals the temperature-dependent variation of damping capacity (indexed by $\tan\delta$) and storage modulus of the NiTi/Ti_3Sn composite, as measured upon heating from −130 °C to 300 °C. The damping peak at about 40 °C corresponds to the reverse B19′ → B2 transformation of the NiTi, which is consistent with the DSC measurement (shown in Fig. 2(b)). As expected, the peak is also associated with a modulus trough due to the dynamic softening of the phase transformation. Besides the transformation-related internal friction peak, the composite also exhibits a rapidly increased high mechanical damping over a wide temperature range at below 0 °C. It is known that the damping capacity of NiTi in martensitic state is practically independent of temperature [11,12]. However, the damping capacity of Ti_3Sn is dependent on the change of temperature [8]. Thus, this high damping capacity of the composite at low temperatures can be ascribed to the contribution of the Ti_3Sn component. The highest $\tan\delta$ of the composite reached is 0.075, which exceeds those of martensitic NiTi SMAs [11,12] and commercial Mn–Cu-based high damping alloys [9,10].

Fig. 3(a) presents an engineering compressive stress–strain curve of the NiTi/Ti_3Sn composite at room temperature. The inset in Fig. 3(a) is the corresponding true stress–strain curve. The composite exhibits about 27.5% plastic strain prior to fracture. The ultimate compressive strength is 1350 MPa. High strain hardening is evident. The yield strength of the composite is about 450 MPa, which is higher than the martensitic NiTi (about 100 MPa) [19] and Mn–Cu (approximately 300 MPa) [9,10] damping alloys. The cylindrical sample was observed to fracture by shear. Fig. 3(b) shows an SEM micrograph of the morphology of a pre-polished lateral surface of the sample after the compression. It is seen that many internal cracks have been formed, mostly propagating through the pre-eutectic Ti_3Sn phase and being arrested by the eutectic structure. This indicates that the soft NiTi component in the eutectic is effective in hindering the propagation of internal cracks and preventing catastrophe failure of the sample, thus enhancing the plasticity of the composite.

In situ synchrotron HEXRD measurements were conducted to investigate the lattice dilation and phase transformation behavior of the composite during deformation. Fig. 4(a) shows a collection of one-dimensional diffraction spectra recorded in the longitudinal direction of the cylindrical sample (the loading direction) at various steps of the deformation process. The *d*-spacing values reflected by the diffraction peaks are the corresponding *d*-spacing values of the planes perpendicular to the loading direction. Upon loading, the B2-NiTi (1 1 0), B19′-NiTi (1 1 1) and Ti_3Sn (2 0 1) peaks are found to shift to lower *d*-spacing values, demonstrating the elastic deformation of all the components in the composite under compression. It is also seen that the intensity of the B19′-NiTi (1 1 1) peak increases whilst the intensity of the B2-NiTi (1 1 0) peak decreases during deformation, which indicates the B2 → B19′ martensitic transformation of the NiTi in the composite.

Fig. 4(b) shows the evolution of the relative integrated intensities of the B2-NiTi (1 1 0) and B19′-NiTi (1 1 1) diffraction peaks, as indicators of the change in volume fractions of the corresponding phases, as functions of the applied strain. The integrated intensity of the B19′-NiTi (1 1 1) peak increases at the expense of that of B2-NiTi (1 1 0) from the very beginning of deformation, indicating the occurrence of the stress-induced B2 → B19′ martensitic transformation. The transformation reaches completion at 7.5% of the applied strain when the B2-NiTi (1 1 0) diffraction peak disappears completely. This observation demonstrates that the stress-induced martensitic transformation (B2 → B19′) of the NiTi plays an important role in the initial deformation of the NiTi/Ti_3Sn composite.

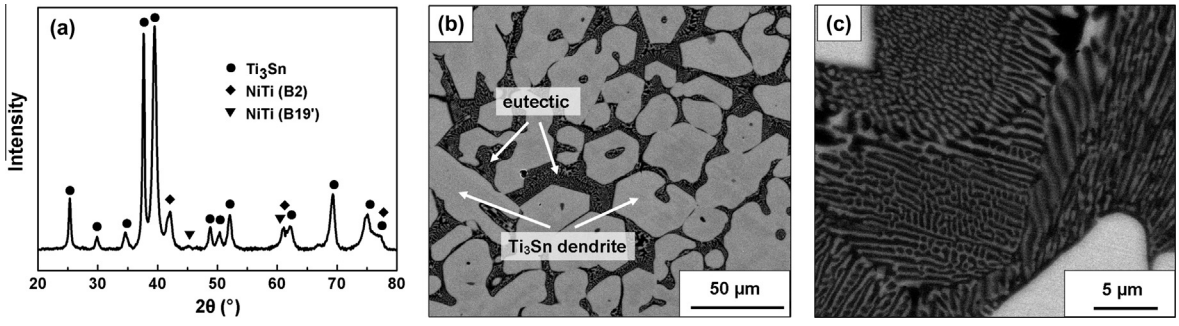

Fig. 1. XRD pattern (a) and SEM backscattered electron micrographs ((b) and (c)) of the NiTi/Ti_3Sn composite.

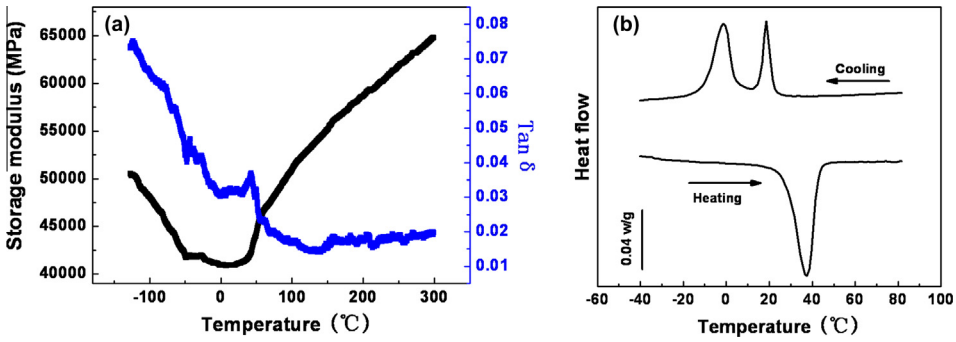

Fig. 2. Functional properties of the NiTi/Ti_3Sn composite. (a) Damping capacity (indexed by tan δ) and storage modulus as a function of temperature during heating process of the composite. (b) DSC curve of the composite.

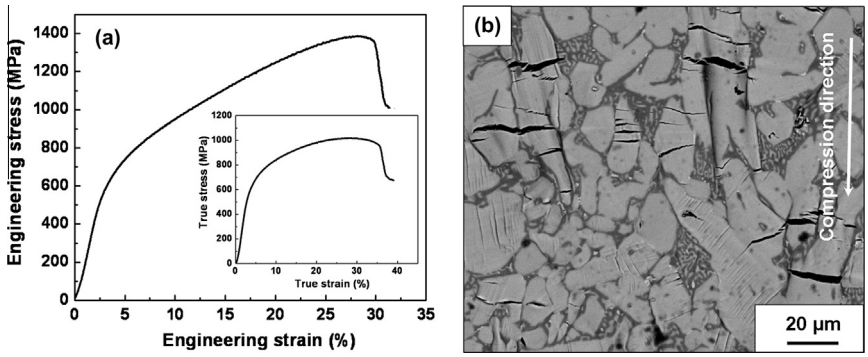

Fig. 3. Mechanical properties of the NiTi/Ti_3Sn composite. (a) Compressive engineering stress–strain curve. The inset is its true stress–strain curve. (b) SEM micrograph of the morphology of the lateral surface of the fracture sample.

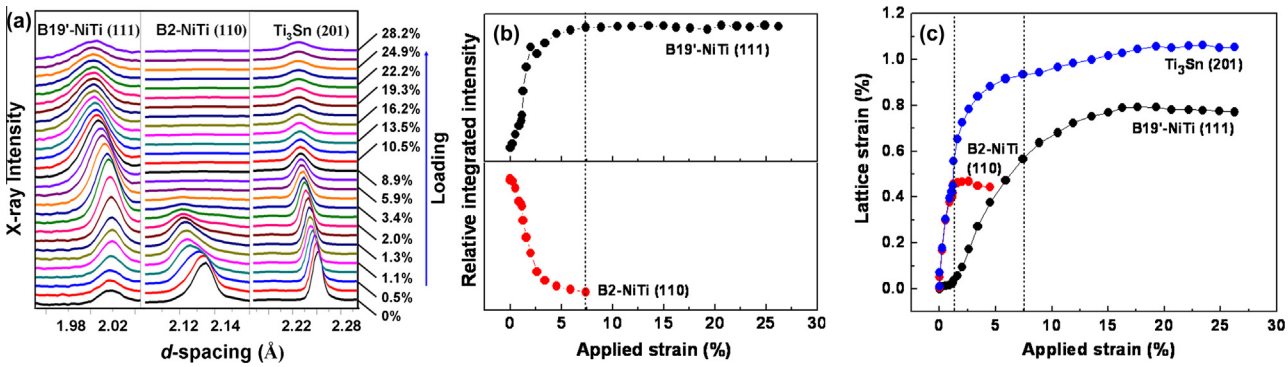

Fig. 4. In situ synchrotron X-ray diffraction analysis of the NiTi/Ti_3Sn composite during compression. (a) One-dimensional diffraction spectra recorded in the longitudinal direction at different levels of applied strain. (b) Relative integrated intensities of the B19′-NiTi (111) and B2-NiTi (110) diffraction peaks, indicating the evolution of the volume fractions of the martensite and austenite phase, plotted as functions of the applied strain. (c) Evolution of the lattice strains of Ti_3Sn (201), B2-NiTi (110) and B19′-NiTi (111) in the direction perpendicular to the loading direction as functions of the applied strain.

Fig. 4(c) shows the lattice strain evolution of Ti_3Sn (201), B2-NiTi (110) and B19′-NiTi (111) in the loading direction as functions of the applied strain. The lattice strains are determined from the HEXRD spectra shown in Fig. 4(a) as $\varepsilon_{hkl} = |d_{hkl} - d_0|/d_0$, where d_0 is the d-spacing of the corresponding planes in the unstressed state. Upon loading, the lattice strains for both Ti_3Sn (201) and B2-NiTi (110) increase rapidly with increasing the applied strain in the initial deformation stage (<1% applied strain), signaling the elastic deformation of these two phases. In contrast, the lattice strain of B19′-NiTi (111) remains low and practically unchanged, which is ascribed to the reorientation deformation of the martensite. At above 1% of the applied strain, the lattice strain of B19′-NiTi (111) increases rapidly whereas that of B2-NiTi (110) remains unchanged at a plateau. This implies the massive transformation of the B2 phase to B19′ phase, whilst the (oriented) B19′ martensite undergoes elastic deformation. It is seen that the elasto-plastic deformation of oriented martensite continues up to 15% of the applied strain. In comparison, the lattice strain of Ti_3Sn (201) reaches an apparent "yield" at 2%, indicating the start of internal micro-cracking. Beyond 15% of the applied strain, neither of the lattice strains of Ti_3Sn (201) and B19′-NiTi (111) change, implying the plastic deformation of the NiTi martensite and internal cracking of Ti_3Sn. Thus, it is clear that the high strain-hardening of the composite over the wide applied strain range (see Fig. 3(a)) originates mainly from the elasto-plastic deformation of the NiTi oriented martensite. Because of the NiTi component, the Ti_3Sn in the composite shows a maximum lattice strain of 1.1%, which is three times of that achieved in pristine Ti_3Sn [14,23]. High

elastic strain implies high load bearing contribution. In this regard, it is apparent that the soft NiTi component with stress-induced martensite transformation helps to prevent stress concentration and strain localization via its transformation deformation whereas the brittle Ti_3Sn intermetallic compound provides the load bearing capacity, thus endowing the composite with enhanced plasticity and high strength.

4. Conclusions

In summary, employing the concept of the transformation-induced plasticity effect in steels, a novel in situ NiTi/Ti_3Sn composite was fabricated. The composite exhibits a high damping capacity together with high strength and large plasticity. The damping capacity of the composite is superior to that of commercial Mn–Cu-based high damping alloys. The Ti_3Sn component primarily provides the strength of the composite, whereas the NiTi component is effective in preventing crack propagation and thus enhances the plasticity.

Acknowledgement

This work was supported by the key program project of National Natural Science Foundation of China (NSFC) (Grant No. 51231008), the National 973 programs of China (Grant No. 2012CB619403), the Australian Research Council (Grant No. DP140103805), and the Key Project of Chinese Ministry of Education (Grant No. 313055). The use of the Advanced Photon Source was supported by the US Department of Energy, Office of Science, and Office of Basic Energy Science, Office of Basic Energy Sciences, under Contract No. DE-AC02-06CH11357.

References

[1] Chung DDL. Structural composite materials tailored for damping. J Alloy Compd 2003;355:216–23.
[2] Lu H, Wang X, Zhang T, Cheng Z, Fang Q. Design, fabrication, and properties of high damping metal matrix composites—a review. Materials 2009;2:958–77.
[3] Ritchie IG, Pan ZL. High-damping metals and alloys. Metall Trans A 1991;22A:607–16.
[4] Schaller R. Metal matrix composites, a smart choice for high damping materials. J Alloy Compd 2003;355:131–5.
[5] Girish BM, Prakash KR, Satish BM, Jain PK, Prabhakar P. An investigation into the effects of graphite particles on the damping behavior of ZA-27 alloy composite material. Mater Des 2011;32:1050–6.
[6] Emadoddin E, Tajally M, Masoumi M. Damping behavior of Al/SiCP multilayer composite manufactured by roll bonding. Mater Des 2012;42:334–8.
[7] Liu G, Tang S, Ren W, Hu J. Effect of thermal cycling on the damping behavior in alumina borate whisker with and without Bi_2O_3 coating reinforced pure aluminum composites. Mater Des 2014;60:244–9.
[8] Vdovychenko OV, Bulanova MV, Fartushna YV, Shcheretsky AA. Dynamic mechanical behavior of intermetallic Ti_3Sn. Scripta Mater 2010;62:758–61.
[9] Tian Q, Yin F, Sakaguchi T, Nagai K. Internal friction behavior of twin boundaries in tensile-deformed Mn–15 at.% Cu alloy. Mater Sci Eng, A 2006;442:433–8.
[10] Zhong Y, Sakaguchi T, Yin F. Effects of transformation twin on Hall–Petch relationship in MnCu alloy. Mater Sci Eng, A 2008;492:419–27.
[11] Li DS, Zhang XP, Xiong ZP, Mai YW. Lightweight NiTi shape memory alloy based composites with high damping capacity and high strength. J Alloys Compd 2010;490. L15-9.
[12] Chen Y, Jiang HC, Liu SW, Rong LJ, Zhao XQ. Damping capacity of TiNi-based shape memory alloys. J Alloys Compd 2009;482:151–4.
[13] Jones PJ, Edington JW. Slip systems in the intermetallic compound Ti_3Sn. Philos Mag 1973;27:393–404.
[14] Hashimoto T, Nakamura M, Takeuchi S. Plastic deformation of Ti_3Sn. Mater Trans, JIM 1990;31:195–9.
[15] Lee CG, Kim SJ, Lee TH, Lee S. Effects of volume fraction and stability of retained austenite on formability in a 0.1C–1.5Si–1.5Mn–0.5Cu TRIP-aided cold-rolled steel sheet. Mater Sci Eng, A 2004;371:16–23.
[16] Chatterjee S, Bhadeshia H. TRIP-assisted steels: cracking of high-carbon martensite. Mater Sci Technol 2006;22:645–9.
[17] Fischer FD, Reisner G, Werner E, Tanaka K, Cailletaud G, Antretter T. A new view on transformation induced plasticity (TRIP). Int J Plast 2000;16:723–48.
[18] Otsuka K, Ren X. Recent developments in the research of shape memory alloys. Intermetallics 1999;7:511–28.
[19] Otsuka K, Ren X. Physical metallurgy of Ti–Ni-based shape memory alloys. Prog Mater Sci 2005;50:511–678.
[20] Hao S, Cui L, Jiang D, Han X, Ren Y, Jiang J, et al. A transforming metal nanocomposite with large elastic strain, low modulus, and high strength. Science 2013;339:1191–4.
[21] Ogata S, Li J, Yip S. Ideal pure shear strength of aluminum and copper. Science 2002;298:807–11.
[22] Lu BC, Xu J. Glass formation of Ti–Ni–Sn ternary alloys correlated with TiNi–Ti_3Sn pseudo binary eutectics. J Non Cryst Solids 2008;354:5425–31.
[23] Wong CR, Fleischer RL. Low frequency damping and ultrasonic attenuation in Ti_3Sn-based alloys. J Mater Res 1994;9:1441–8.